

# Functionalization of Graphene Oxide Films with Au and MoO<sub>x</sub> Nanoparticles as Efficient *p*-Contact Electrodes for Inverted Planar Perovskite Solar Cells

Sumit S. Bhosale, Efat Jokar, Amir Fathi, Cheng-Min Tsai, Chi-Yung Wang, and Eric Wei-Guang Diao\*

A graphene oxide (GO) film is functionalized with metal (Au) and metal-oxide (MoO<sub>x</sub>) nanoparticles (NPs) as a hole-extraction layer for high-performance inverted planar-heterojunction perovskite solar cells (PSCs). These NPs can increase the work function of GO, which is confirmed with X-ray photoelectron spectra, Kelvin probe force microscopy, and ultraviolet photoelectron spectra measurements. The down-shifts of work functions lead to a decreased level of potential energy and hence increased  $V_{oc}$  of the PSC devices. Although the GO-AuNP film shows rapid hole extraction and increased  $V_{oc}$ , a  $J_{sc}$  improvement is not observed because of localization of the extracted holes inside the AuNP that leads to rapid charge recombination, which is confirmed with transient photoelectric measurements. The power conversion efficiency (PCE) of the GO-AuNP device attains 14.6%, which is comparable with that of the GO-based device (14.4%). In contrast, the rapid hole extraction from perovskite to the GO-MoO<sub>x</sub> layer does not cause trapping of holes and delocalization of holes in the GO film accelerates rapid charge transfer to the indium tin oxide substrate; charge recombination in the perovskite/GO-MoO<sub>x</sub> interface is hence significantly retarded. The GO-MoO<sub>x</sub> device consequently shows significantly enhanced  $V_{oc}$  and  $J_{sc}$ , for which its device performance attains PCE of 16.7% with great reproducibility and enduring stability.

## 1. Introduction

Lead-halide perovskite (PSK) solar cells (PSCs) have emerged as the most promising photovoltaic devices because of the rapid progress in their device performance with a potential to scale up to a production level.<sup>[1]</sup> Based on an ambipolar charge-transport property and a large diffusion length for electrons


and holes in a perovskite crystal, thin-film perovskite solar cells with a planar-heterojunction (PHJ) configuration have been developed.<sup>[2,3]</sup> In the PHJ structure, the perovskite layer serves as a light absorber between the two electrodes to transport electron and hole carriers separately. The PHJ device has a simplified fabrication with satisfactory performance without high-temperature annealing, such as is required to fabricate mesoporous layers.<sup>[4,5]</sup> PHJ devices exist of two types—either a regular (*n-i-p*) or an inverted (*p-i-n*) configuration.<sup>[2,6,7]</sup> Various materials have been used as the hole-extraction layer (HEL) or electron-extraction layer in these device configurations.<sup>[7–10]</sup> The inverted PHJ devices are particularly intriguing because charge separation would first occur at the *p*-contact HEL/perovskite interface that facilitates the transport of the hole carriers.<sup>[2–8,11]</sup> A suitable HEL material for an inverted PHJ device should have the following characteristics: i) effective hole mobility, ii) a compatible energy level matching the valence-band (VB) level of a perovskite, iii) excellent film formation

from a solution-based process, iv) great transparency in the visible and near infrared regions, and v) cost-effective production of the material itself. Carbon-based nanomaterials such as carbon nanotubes,<sup>[12]</sup> graphene oxide (GO),<sup>[13,14]</sup> and reduced graphene oxide (rGO)<sup>[15]</sup> have recently been reported as an efficient HEL for an inverted PHJ PSC.

Chemically synthesized GO is a graphene sheet containing, on its 2D carbon-skeleton network, functional groups such as hydroxyl, epoxide, carboxylic, and carbonyl. The presence of these oxygen groups on a 2D network of the GO surface enhances its hydrophilic properties; GO is thus well dispersed in water or polar solvents, which is regarded as an advantage of GO, especially in studies of the composite of GO with other nanomaterials.<sup>[14–17]</sup> Differing from an HEL of polymer type such as poly(3,4-ethylenedioxythiophene) polystyrene sulfonate with acidic and hygroscopic properties that cause poor enduring stability of the devices, PSC consisting of GO and its derivatives as HEL have shown great device performance and enduring stability.<sup>[13,15,18]</sup> For GO as an effective HEL, the work function

S. S. Bhosale, Dr. E. Jokar, A. Fathi, C.-M. Tsai, C.-Y. Wang, Prof. E. W.-G. Diao  
Department of Applied Chemistry and Institute of Molecular Science  
National Chiao Tung University  
1001 Ta-Hsueh Rd., Hsinchu 30010, Taiwan  
E-mail: diau@mail.nctu.edu.tw

Prof. E. W.-G. Diao  
Center for Emergent Functional Matter Science  
National Chiao Tung University  
1001 Ta-Hsueh Rd., Hsinchu 30010, Taiwan

 The ORCID identification number(s) for the author(s) of this article can be found under <https://doi.org/10.1002/adfm.201803200>.

DOI: 10.1002/adfm.201803200

(WF =  $-5.0$  eV vs vacuum) is, however, not quite near the VB of perovskite ( $-5.4$  eV for  $\text{MAPbI}_3$ ).<sup>[14]</sup> Previous reports<sup>[19–21]</sup> indicate that a deposition of metal or metal-oxide nanoparticles (NPs) on graphene can alter its work function because the interaction of those NP with graphene might cause *p* or *n*-doping on the graphene sheets. Functionalization of GO with NP deposited on its surface should, accordingly, be a simple way to alter the WF for GO. Modification of GO to match the energy level as HEL for PSC is hence one of our goals to improve the power conversion efficiency (PCE) of the devices.

Previous reports have stated that the WF of GO can be altered on attaching organic molecules, depositing metal or metal-oxide NPs,<sup>[20,22,23]</sup> grafting organic molecules,<sup>[24,25]</sup> and exposing to an inorganic salt.<sup>[26]</sup> Various metal chlorides were used as *p*-dopants to modify the WF of the graphene nanosheets.<sup>[19]</sup> Moreover, metal oxides, such as molybdenum oxide ( $\text{MoO}_x$ ) or tungsten oxide ( $\text{WO}_x$ ), can also functionalize graphene and alter its WF.<sup>[20,21]</sup> In the present work, our purpose is to apply this idea to increase the WF of GO as HEL to enhance  $V_{oc}$  for a GO-based inverted planar PSC. We chose both gold (Au) and  $\text{MoO}_x$  NP to deposit on the surface of GO because they have either a large work function (Au) or a deep valence band ( $\text{MoO}_x$ ).

A thin GO film can serve as an efficient HEL for an inverted planar PSC.<sup>[13,15]</sup> Irrespective of the rapid hole-extraction feature of GO, the localization of extracted holes on the GO surface acts as a source of charge recombination (CR). One approach was to reduce those localized oxide sites with a reducing agent to form rGO so that the holes extracted by rGO became delocalized to retard the charge recombination and to enhance the device performance significantly.<sup>[15]</sup> A compromise of using rGO as HEL for PSC was that the hole-extraction periods might become much longer than those using GO. In the present work, we show how GO can be functionalized using metal or metal-oxide NP to solve the bottleneck problem of retarded charge recombination. We chose NP of both gold and  $\text{MoO}_x$  so that they can increase both the WF of GO and the  $V_{oc}$  of the device. For the GO-AuNP composite, there is an additional plasmonic effect to enhance the exciton contribution in the band edge of the incident photon-to-current conversion efficiency (IPCE) spectrum, but it failed to improve the overall device performance because charges trapped inside the AuNP enhanced the charge recombination and decreased the charge transport. In contrast, for the GO- $\text{MoO}_x$  composite as HEL for PSC, we observed a significant improvement of  $V_{oc}$  compared with that of the GO device, which we attribute to the effects of reducing the potential level of WF and retarding charge recombination due

to delocalization of the holes via the functionalization of GO nanosheets with the  $\text{MoO}_x$  NP. The devices made of this GO- $\text{MoO}_x$  composite as HEL attained the best performance, with PCE of 16.7%, which is much superior to that of the reference cell in the absence of  $\text{MoO}_x$  NP on the surface of GO, for which PCE = 14.4%.

## 2. Results and Discussion

GO was synthesized with the Hummers process<sup>[15]</sup>; Au or  $\text{MoO}_x$  NP on GO was deposited via spin-coating of their salt solutions, chloroauric acid for Au, and molybdenum bronze for  $\text{MoO}_x$ .<sup>[19,27]</sup> For the formation of the GO-Au films, the adsorbed gold cations on the surface of GO were reduced at  $100^\circ\text{C}$  by the GO itself to form Au nanoparticles. The GO modification with nanoparticles was confirmed with X-ray photoelectron spectra (XPS). The C 1s core-level spectra were deconvoluted into five components (Figure 1), which are attributed to functional groups C=C, C–C, C–O, C=O, and O–C=O, respectively. The fractions of carbon functional groups of varied types are listed in Table 1. The XPS signals of Au 4f and Mo 3d are depicted in Figure S1 (Supporting Information), to confirm that the Au and  $\text{MoO}_x$  nanoparticles are present on both GO films. The XPS data show that the presence of Au and  $\text{MoO}_x$  NP significantly altered the relative intensities of C=C and C=O signals. In rGO, the oxygen-containing functional groups can be reduced to C=C via a reducing agent to improve the conductivity of GO. Both NPs hence played a role to reduce the amount of C=O functional group so that the fraction of the C=C functional group increased significantly. These functionalized GO films should thus have some characteristics like those of an rGO film, as we reported previously.<sup>[15]</sup>

Figure 2 shows the image results obtained from measurements using the Kelvin-probe force microscope (KFM), which provide evidence of *p*-doping characteristics of the functionalized GO films. The GO film with more *p*-doping character via NP functionalization would show a lower potential because of the bias voltage applied to the tip of the KFM. From the distribution plots of the contact potential difference (CPD) shown in Figure S2 (Supporting Information), we observed a decreased CPD with the trend  $\text{GO-MoO}_x > \text{GO-AuNP} > \text{GO}$ , indicating that the effect of *p*-doping should have the same trend for the corresponding hybrid films. The measured root-mean-square roughnesses of bare GO, GO-AuNP, and GO- $\text{MoO}_x$  were 0.15, 0.21, and 0.30 nm, respectively. As one can discern

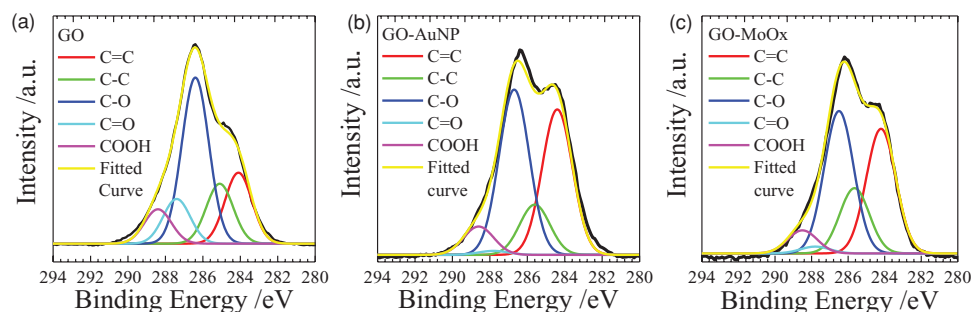


**Figure 1.** C 1s XPS spectra of a) GO, b) GO-AuNP, and c) GO- $\text{MoO}_x$  samples.

**Table 1.** Analysis of C 1s binding energies and atomic percentages of carbon functional groups in GO, GO-AuNP, and GO-MoO<sub>x</sub>.

Sample	Proportion of carbon 1s group				
	C=C	C-C	C-O	C=O	O-C=O
GO	18.9	15.9	44.2	11.9	9.1
GO-AuNP	36.9	12.7	42.02	1.0	7.2
GO-MoO <sub>x</sub>	34.4	18.02	39.3	1.9	6.3

in Figure 2, the surface of the GO-MoO<sub>x</sub> sample was rougher than those of GO and GO-AuNP films.

According to a previous report,<sup>[20]</sup> the formation of a surface negative dipole due to electron transfer from graphene to the deposited MoO<sub>x</sub> NP increased the work function of graphene (Scheme 1). The existence of gap states in MoO<sub>x</sub> induced by oxygen vacancies greatly lowered the barrier for hole injection at the MoO<sub>x</sub>/graphene interface. Charge transport toward a metal ion is hence a spontaneous process. Figure S3a–d (Supporting Information) shows ultraviolet photoelectron spectra (UPS) of GO, GO-AuNP, GO-MoO<sub>x</sub>, and MoO<sub>x</sub> in regions of large and small kinetic energy. These results indicate that the valence-band maximum in the region of large kinetic energy decreases on introducing Au and MoO<sub>x</sub>. The potential-energy level of the GO as prepared versus the vacuum level is –5.01 eV, which is shifted slightly downward on adding the AuNP and MoO<sub>x</sub> on the GO film. The potential levels of the GO-AuNP and GO-MoO<sub>x</sub> composites are –5.05 and –5.08 eV, respectively.

Inverted PHJ perovskite solar cells were fabricated based on device configuration ITO/GO-*x*NP/MAPbI<sub>3</sub>/phenyl-C61-butyric acid methyl ester (PCBM)/BCP/Ag, shown in Scheme 1. A perovskite layer was deposited with a typical anti-solvent method<sup>[28]</sup> followed by a solvent-annealing (SA) treatment.<sup>[29]</sup> Chlorobenzene served as an anti-solvent that introduced supersaturation to form a uniform perovskite film. Post-SA under dimethylformamide (DMF) vapor led to growth of PSK

nanocrystals with larger grains. Figure S4 (Supporting Information) shows top-view scanning electron microscope (SEM) images for all PSK films grown on GO-based HEL, for which pin-hole-free, close-packed and uniform perovskite films of the HEL of all types were produced. The crystal structures of the grown perovskite films were investigated with X-ray diffraction (XRD) and the data are shown in Figure S5 (Supporting Information); no difference was found for the morphology and crystallinity of PSK grown on various GO-based HELs.

The device performances were first optimized for varied concentrations of Au and MoO<sub>x</sub> precursors; the corresponding results are shown in Figure S6 and Tables S1 and S2 (Supporting Information). Figure 3a shows the photovoltaic performances and Figure 3b the corresponding IPCE spectra for the best cells made with varied HEL, GO, and NP-doped GO-based devices. The photovoltaic parameters of the corresponding devices are summarized in Table 2. For the GO device, we obtained PCE of 14.4%, which is substantially greater than that reported by Wu et al., PCE = 12.4%.<sup>[14]</sup> The GO-MoO<sub>x</sub> device showed a greater photovoltaic performance (PCE = 16.7%) that is due to improvement of both *V*<sub>oc</sub> and *J*<sub>sc</sub>. In contrast, *V*<sub>oc</sub> was improved for the GO-AuNP device, whereas *J*<sub>sc</sub> was decreased and the overall device performance attained PCE of 14.6% for the GO-AuNP device. The calculated *J*<sub>sc</sub> values from the IPCE spectra (Figure 3b) are consistent with the *J*<sub>sc</sub> values obtained from the *J*–*V* curves (Figure 3a). MoO<sub>x</sub> apparently plays an important role in enhancing the device performance to attain the level as for the rGO-based PSC,<sup>[15]</sup> but the operational mechanisms for the devices of the two types differ, as detailed in the following section.

An improved *V*<sub>oc</sub> on introducing metal or metal oxide was confirmed on testing 35 devices of each type under the same experimental conditions; the corresponding photovoltaic parameters are listed in Tables S3–S5 (Supporting Information). Figure 4 compares the distributions of *J*<sub>sc</sub>, *V*<sub>oc</sub>, fill factor, and PCE for these devices with GO-based HEL of various types. Mean PCE/% 13.6 ± 0.8, 12.8 ± 1.1, and 15.4 ± 0.8 were

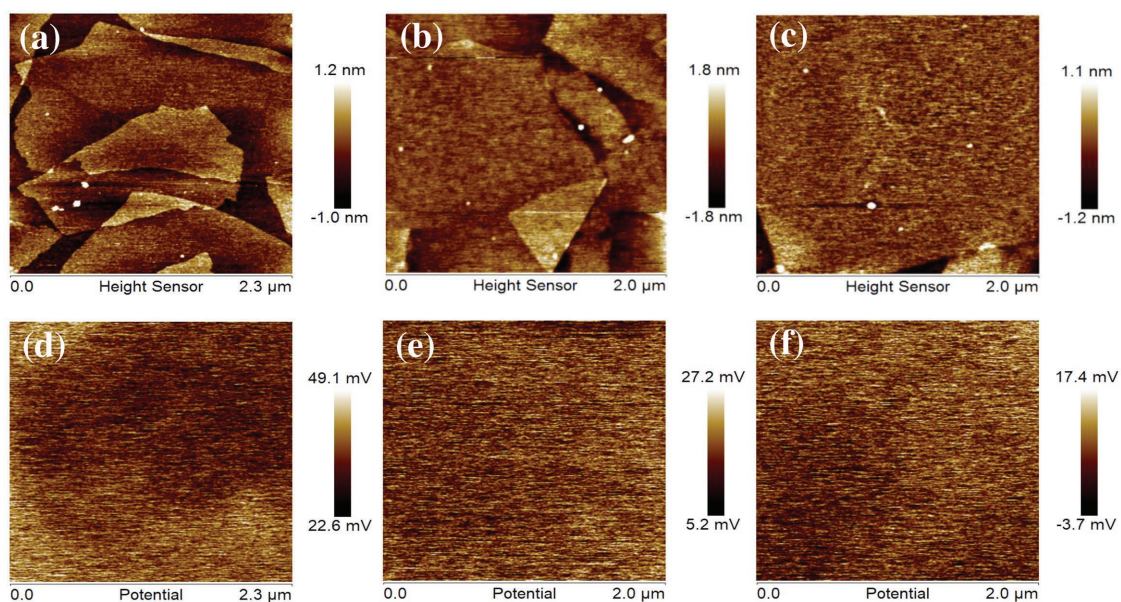
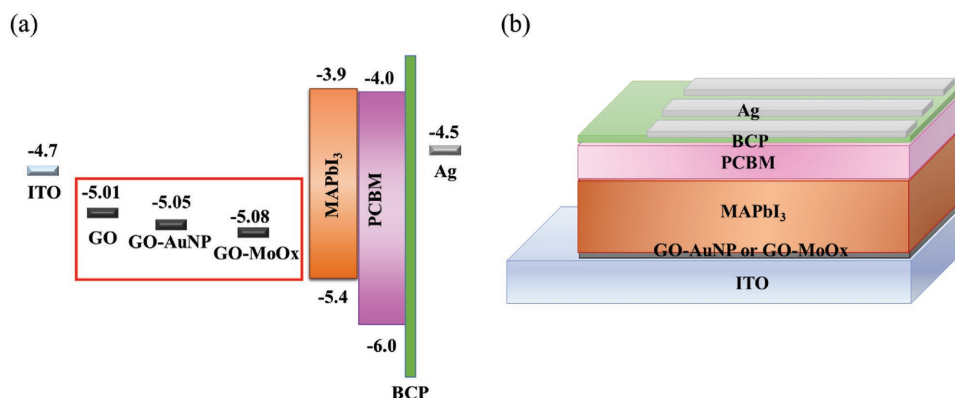


**Figure 2.** Atomic force microscopy and KFM images of a,d) GO, b,e) GO-AuNP, and c,f) GO-MoO<sub>x</sub> films.



**Scheme 1.** a) Potential-energy diagram of GO, GO-AuNP, and MoO<sub>x</sub>-NP layers (shown in a red box) with other components comprising the device structure of an inverted PHJ perovskite solar cell shown in (b).

obtained for devices with the HEL made of GO, GO-AuNP, and GO-MoO<sub>x</sub>, respectively. Both GO and GO-MoO<sub>x</sub> devices show almost no hysteresis whereas the GO-AuNP device indicates a slight effect of hysteresis in the  $J$ - $V$  scans shown in Figure S7 (Supporting Information). The  $J$ - $V$  hysteresis behavior observed only for the GO-AuNP device might be attributed to the slow transient capacitive current, dynamic trapping and detrapping processes, and band bending due to ion migrations or ferroelectric polarization.<sup>[30]</sup> The charges trapping inside AuNP may cause the transport time of the GO-AuNP device become much longer than those of GO-MoO<sub>x</sub> and GO devices. Then extraction and transporting in HEL for GO-AuNP devices were not efficient and might cause unbalance between extraction of holes and electrons that leads to the observed effect of hysteresis.<sup>[31]</sup> As will be discussed in the following, we expect that the presence of hysteresis in GO-AuNP devices is due to the effect of trapping of the charges inside AuNP at the interface of HEL/PSK.

These highly efficient devices are stable, which can be recognized from the endurance test over 1500 h shown in Figure S8 (Supporting Information). The PCE of these GO-based devices maintains more than 80% of their initial efficiencies up to 1500 h for devices without encapsulation and under ambient conditions (25 °C and 30% humidity). The statistical data show clearly that  $V_{oc}$  was improved for devices made of NP-modified GO films as HEL, but the GO-AuNP devices showed smaller

$J_{sc}$  values than those of the standard GO devices and the GO-MoO<sub>x</sub> devices. The decreased  $J_{sc}$  of the former device is attributed to the trapping of charges in the AuNP that facilitates charge recombination between AuNP and perovskite.<sup>[32]</sup> To reveal an exact reason for the improved device performance of NP-modified GO-based devices, we recorded steady-state spectra of photoluminescence (PL) and performed time-correlated single-photon counting (TCSPC) measurements for samples containing the hybrid GO-NP as the HEL and the perovskite layers.

Bilayer samples were prepared with the perovskite layer deposited on either an ITO/GO or an ITO/GO-metal (or an ITO/GO-metal-oxide) substrate; the reference sample is the perovskite deposited on the ITO substrate. Compared with the PSK sample on ITO, GO, or GO-AuNP/GO-MoO<sub>x</sub> quenched the PL of PSK significantly (Figure 5a). As shown in the inset of Figure 5a, the effect of PL quenching is more pronounced for the GO surface treated with AuNP and MoO<sub>x</sub> than that of pristine GO; the PL intensities of PSK on separate underlayers show an order ITO/PSK > ITO/GO/PSK > ITO/GO-AuNP/PSK ~ ITO/GO-MoO<sub>x</sub>/PSK. This result indicates that, to quench the PL intensity effectively, the functionalization of the GO surface with AuNP and MoO<sub>x</sub> has a hole-extraction characteristic better than the GO layer alone. The PL intensity is regarded as an indirect marker for the lifetimes of the excitons produced in

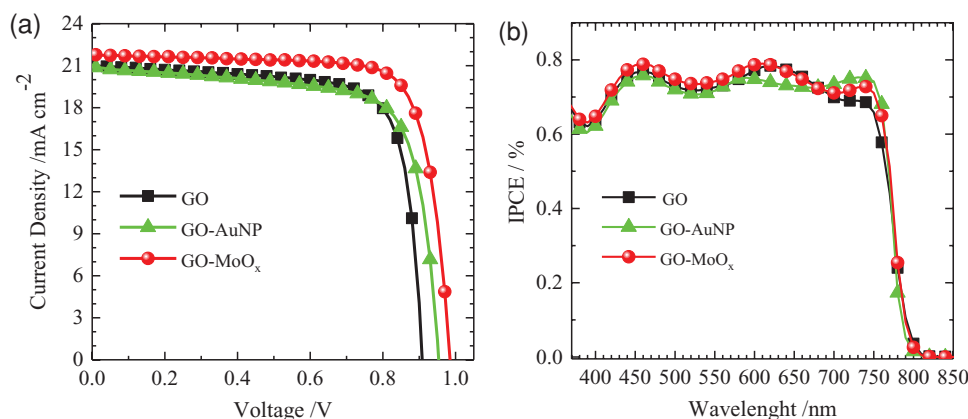


**Figure 3.** a)  $J$ - $V$  curves and b) IPCE spectra of devices fabricated using GO, GO-AuNP, and GO-MoO<sub>x</sub> as HEL.

**Table 2.** Photovoltaic parameters of inverted planar heterojunction perovskite solar cells fabricated with varied *p*-type HEL materials under simulated AM-1.5G illumination (power density 100 mW cm<sup>-2</sup>).

HEL <sup>a)</sup>	$J_{sc}$ [mA cm <sup>-2</sup> ]	$V_{oc}$ [V]	FF	PCE [%]
GO	21.0	0.913	0.751	14.4 (13.6 ± 0.8)
GO-AuNP	20.8	0.961	0.726	14.6 (12.8 ± 1.1)
GO-MoO <sub>x</sub>	21.8	0.990	0.773	16.7 (15.4 ± 0.8)

<sup>a)</sup>Hole-extraction layers (HELs) were prepared with varied GO-modified films for inverted planar devices with the device structure shown in Scheme 1b.

these samples, but direct evidence is provided by the PL decay measurements of these samples with the TCSPC technique.

The normalized transient PL decays of the corresponding samples taken under conditions  $\lambda_{ex} = 635$  nm and  $\lambda_{PL} = 770$  nm are shown in Figure 5b, which exhibit a trend of decay feature similar to that of the PL quenching feature shown in Figure 5a. All PL transients were fitted with a triexponential decay function, except that of pristine PSK sample with a biexponential decay function; the fitted time coefficients and the corresponding relative amplitudes are summarized in Table S6 (Supporting Information). The trend of average PL lifetimes ( $\tau_{PL}$ ) of the samples shows the order ITO/PSK > ITO/GO/PSK > ITO/GO-AuNP /PSK ~ ITO/GO-MoO<sub>x</sub>/PSK. Assuming that all PL quenches are due to the effect of hole extraction, we evaluated the hole-extraction times ( $\tau_h$ ) (Table S6, Supporting Information) to compare the ability of hole extraction for all three samples; the trend of rate coefficients ( $1/\tau_h$ ) for hole extraction

shows that doping of GO with MoO<sub>x</sub> and AuNP increases the rate of hole extraction.

Based on our previous work,<sup>[15]</sup> the rapid extraction of holes in the GO/PSK interface is due to the existence of oxygen-containing functional groups. As shown in Figure 1 and Table 1, the XPS results indicate, however, that doping Au and MoO<sub>x</sub> nanoparticles on GO decreased the amount of oxygen-containing functional groups, similarly to the characteristic of rGO. For the case of rGO, the rate of hole extraction was decreased relative to that of GO. The enhanced hole extraction in the hybrid GO/NP systems is thus due to the *p*-doping effect of both AuNP and MoO<sub>x</sub> NP. The AuNP on the surface of GO facilitates rapid extraction of holes, but the extracted holes were also stabilized inside the AuNP; the subsequent transfer of holes to ITO hence becomes slowed, shown schematically in **Scheme 2a**. As a result, the localized holes trapped inside AuNP could lead to CR; the effect of CR results in a decreased  $J_{sc}$  of the device. In contrast, in the case of the GO-MoO<sub>x</sub> film, the hole extraction from PSK to GO-MoO<sub>x</sub> was rapid because of *p*-doping, but the extracted holes were not localized; they can be efficiently transferred to ITO so that CR was significantly retarded (Scheme 2b).

The mechanism proposed in Scheme 2 was confirmed with the transient photoelectric measurements under six bias light intensities using a technique reported elsewhere<sup>[15,33]</sup>; the results appear in **Figure 6**. For the transient photocurrent decays measured under short-circuit conditions (Figure 6a), we observed rapid transient decays for all devices independent of the bias light intensity (Figure S9a–c, Supporting Information). This capacitive behavior is typical of a *p-i-n* photodiode,

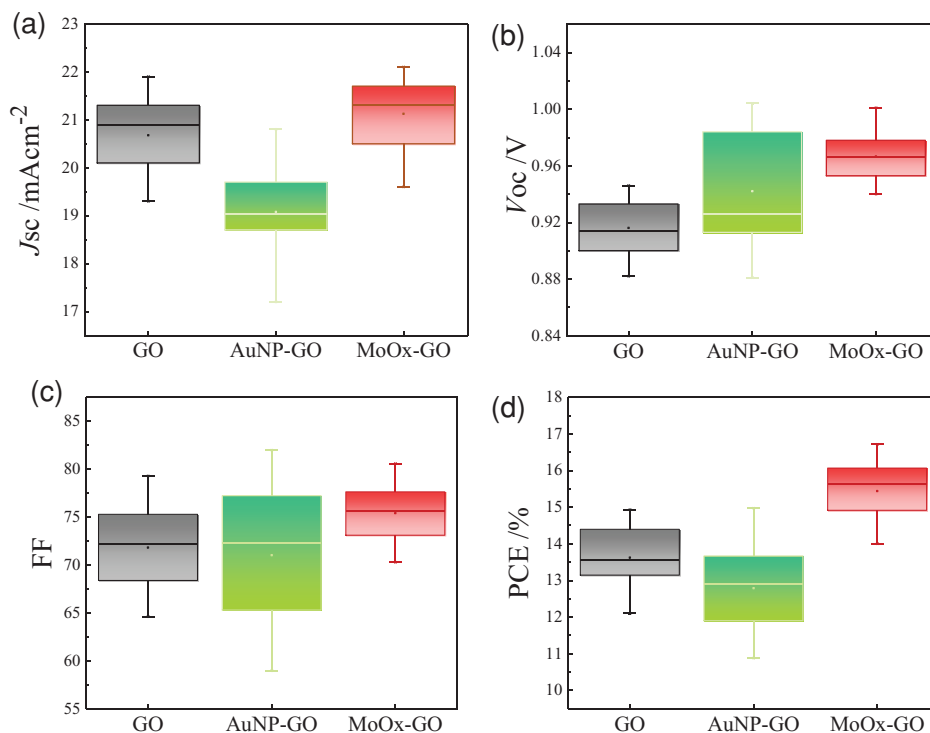


**Figure 4.** Boxplots of photovoltaic parameters a)  $J_{sc}$ , b)  $V_{oc}$ , c) FF, and d) PCE for devices made of GO, GO-AuNP, and GO-MoO<sub>x</sub> as HEL.

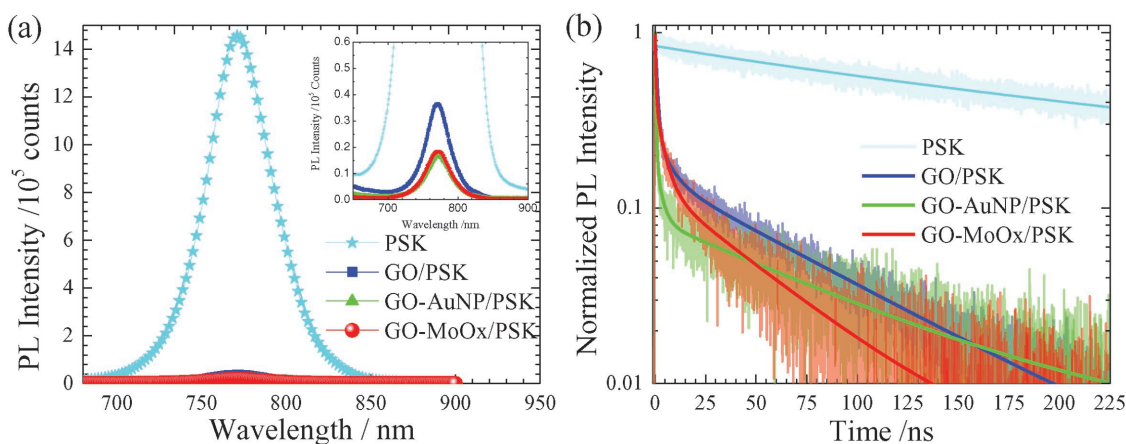


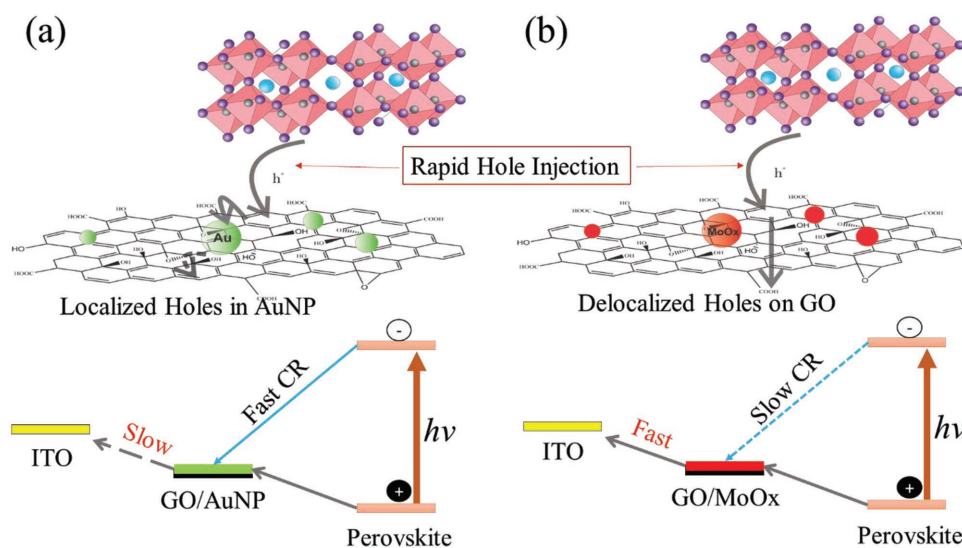
**Figure 5.** a) Photoluminescence (PL) spectra and b) transient PL decay profiles of PSK on ITO and on HEL-GO, GO-AuNP, or GO-MoO<sub>x</sub>.

for which charge accumulation in the HEL/PSK interface becomes a bottleneck. The photocurrent transients hence gave invariably constant decay coefficients ( $\tau_c$ ) with the order GO-AuNP > GO-MoO<sub>x</sub> > GO on a time scale  $\approx 200$  ns, which is equal to the resistance-capacitance (RC) time constants of the devices in the HEL/PSK interface that do not directly correlate to the variation of  $J_{sc}$  of the devices. Charge-collection times of all devices are hence RC limited; the rate of hole propagation from the GO or hybrid GO layer to the ITO substrate should conform to the same trend, GO > GO-MoO<sub>x</sub> > GO-AuNP. Because of the charges trapped inside the AuNP, the transport interval of the GO-AuNP device hence became much longer than those of GO-MoO<sub>x</sub> and GO devices. In contrast, for transient photovoltage decays measured under open-circuit conditions, the charge recombination times were well resolved, as the raw data show in Figure S10a-c (Supporting Information) for the GO, GO-AuNP, and GO-MoO<sub>x</sub> devices, respectively. All photovoltage decay profiles were fitted with a single-exponential decay function with values of the CR decay coefficient ( $\tau_r$ ) shown in Figure 6b, for which the  $\tau_r$  values of

the GO-AuNP device are smaller than those of the other two devices. The question remained is why the  $V_{oc}$  showed a trend for devices GO-MoO<sub>x</sub> > GO-AuNP > pristine GO but  $\tau_r$  showed a trend GO-MoO<sub>x</sub> > pristine GO > GO-AuNP? The larger  $V_{oc}$  for the GO-AuNP device than for the pristine GO device was puzzling. We speculate that it might be due to the position of WF, for which the GO-AuNP film is shifted downward by 0.04 eV compared to that of GO film (Scheme 1). Our results clearly indicate that the CR times are much greater for the GO-MoO<sub>x</sub> device than for the GO and the GO-AuNP devices, consolidating our mechanism illustrated in Scheme 2.

### 3. Conclusion

We report the development of GO films functionalized with AuNP and MoO<sub>x</sub> NP as HEL for inverted planar perovskite solar cells. GO-AuNP and GO-MoO<sub>x</sub> films were prepared with spin-coating of gold (III) chloride trihydrate (HAuCl<sub>4</sub>·3H<sub>2</sub>O) and molybdenum bronze solutions on GO/ITO substrates,



**Scheme 2.** Schematic representation of the mechanism of hole transport in a) GO-AuNP and b) GO-MoO<sub>x</sub> devices.

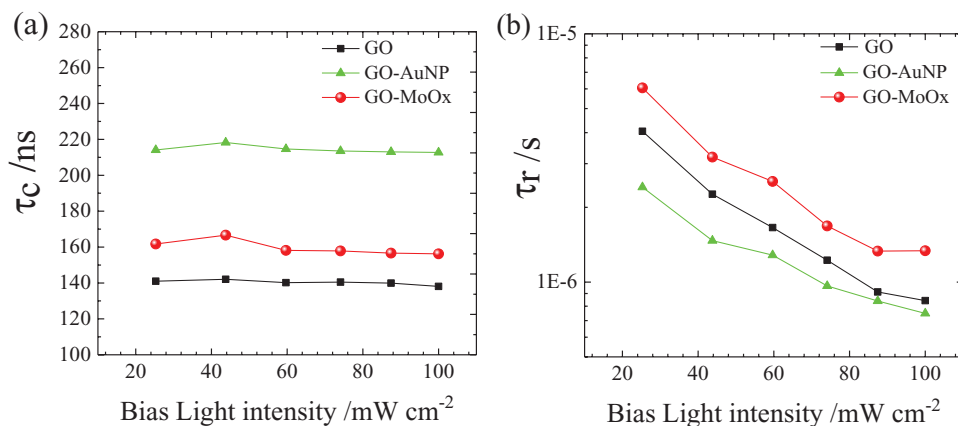


**Figure 6.** a) Time coefficient  $\tau_c$  for charge collection and b)  $\tau_r$  for charge recombination as a function of bias light intensity for the GO, GO-AuNP, and GO-MoO<sub>x</sub> devices.

respectively. The functionalization of GO films with AuNP and MoO<sub>x</sub> increases the work function of GO, which results in an enhanced  $V_{oc}$  for both AuNP and MoO<sub>x</sub> devices. Moreover, the hole extraction from PSK to HEL became more rapid for the NP-modified hybrid GO films than for the pristine GO film because of the effect of *p*-doping of the former films. The extracted holes were trapped inside AuNP (localized holes) so that further hole transport into the ITO substrate became slower for the AuNP-GO device than for the GO-based and the GO-MoO<sub>x</sub> devices. As a result, the GO-AuNP device showed a greater effect of hysteresis and rapid charge recombination that produces a device performance (PCE 14.6%) comparable with that of the GO-based device (PCE 14.4%). In contrast, the GO-MoO<sub>x</sub> device helps to even the hole distribution, forming delocalized holes in the 2D GO framework to retard charge recombination and enhance both  $J_{sc}$  and  $V_{oc}$  to produce a device performance attaining PCE 16.7%. We conclude that the functionalization of a GO film with MoO<sub>x</sub> NP as HEL has an effective *p*-doping effect to lower the work function of GO and to retard charge recombination in the PSK/GO interface for the improved device performance that we report herein.

#### 4. Experimental Section

**Synthesis of Graphene Oxide:** GO was synthesized using the Hummers method that was explained previously.<sup>[11,13]</sup> For the preparation of HEL, GO solution (1 mg mL<sup>-1</sup> in DMF) was spin-coated on the ITO substrates (treated with UV-O<sub>3</sub> for 20 min) at 4000 rpm for 40 s, followed by annealing at 125 °C for 10 min. To dope a GO film with metal nanoparticles, we used reduction in situ from a salt solution. HAuCl<sub>4</sub> solution (0.5 × 10<sup>-3</sup> M) was spin-coated on a GO/ITO substrate at 3000 rpm for 30 s; the substrate was then washed with ethanol to remove excess metal salt. The washed substrate was annealed at 100 °C for 10 min.

GO-MoO<sub>x</sub> nanoparticles were prepared on spin-coating of molybdenum bronze solution (0.1 mg mL<sup>-1</sup> in ethanol) on GO/ITO. The synthesis of molybdenum bronze is reported elsewhere.<sup>[27]</sup>

**Device Fabrication:** After deposition of a GO-based HEL, the substrates were transferred to a glove box. Perovskite solution (50%) was prepared on mixing the synthesized CH<sub>3</sub>NH<sub>3</sub>I powder with PbI<sub>2</sub> (Alfa Aesar) at molar ratio 1:1 in anhydrous DMF at 70 °C overnight. A PSK solution

was first spin-coated on the ITO/GO substrate at 5000 rpm (torsion rate 10 000 rpm s<sup>-1</sup>). With delay period of 5 s, chlorobenzene was dropped onto the substrate to promote rapid nucleation, followed by annealing at 100 °C for 2 min. The films were subjected to solvent annealing: the perovskite film was kept under DMF vapor at 100 °C for 10 min. A PCBM solution in chlorobenzene (20 mg mL<sup>-1</sup>) was spin-coated on the PSK layer at 1000 rpm (torsion rate: 1000 rpm s<sup>-1</sup>) for 30 s as an electron-transport layer. Ag (100 nm) was deposited with thermal evaporation in a vacuum system (pressure 5 × 10<sup>-6</sup> Torr).

**Characterization of Materials and Devices:** A field-emission SEM (Hitachi SU8010) and an atomic-force microscope (VT SPM, SII Nanotechnology Inc.) were used to investigate the morphology and structure of the samples. The surface potential was measured under ambient conditions, employing Pt-coated Si probes (CSC17/Cr-Au) with force constant 0.18 N m<sup>-1</sup> and a tip radius typically about 35 nm. The XRD patterns of the thin films coated on the ITO substrates were obtained with an X-ray diffractometer (Bruker AXS, D8 Advance, Cu K $\alpha$  irradiation,  $\lambda = 154.18$  pm). The current density–voltage characteristics of devices were recorded with a digital source meter (Keithley 2400) under one-sun illumination (AM 1.5G, 100 mW cm<sup>-2</sup>) with a solar simulator (XES-40S1, SAN-E1), calibrated with a silicon diode and a KG-5 filter to decrease the mismatch of the spectrum. The spectra of IPCE were recorded with a system comprising a Xe lamp (A-1010, PTI, 150 W) and a monochromator (PTi). The absorption spectra of the thin film and solution samples were recorded with a spectrophotometer (JASCO V-570). The PL spectra were recorded in a range 650–900 nm with excitation at 635 nm (LDH-635, PicoQuant). The PL transients were recorded with a TCSPC system (Fluotime 200, PicoQuant, excitation at 635 nm) from a picosecond pulsed-diode laser (LDH-635, PicoQuant, full width at half maxima  $\approx$ 70 ps). The repetition rate of the laser used for all experiments was 0.5 MHz; the pulse energy was 1 nJ cm<sup>-2</sup>; the beam size was expanded to 1.5 mm × 3.5 mm. XPS were recorded (Thermo K-ALPHA Surface Analysis) for graphene oxide and modified graphene oxide. UPS were recorded with samples prepared on a silicon wafer and FTO/TiO<sub>2</sub> substrates at beamline 24A of Taiwan Light Source in National Synchrotron Radiation Research Center (NSRRC). For UPS, an excitation source with photon energy 36.4 eV was used; the samples were biased at –5.0 V to avoid the low-energy secondary cut-off signals of the samples. All experiments were calibrated with the Fermi edge of a clean Au surface.

#### Supporting Information

Supporting Information is available from the Wiley Online Library or from the author.

## Acknowledgements

The Taiwan Ministry of Science and Technology (MOST) (MOST 107-3017-F009-003, MOST 105-2119-M-009-MY3, and MOST 106-2119-M-009-001) supported this work. The authors thank support from the Center for Emergent Functional Matter Science of National Chiao Tung University through the Featured Areas Research Center Program within the framework of the Higher Education Sprout Project by the Taiwan Ministry of Education. The National Synchrotron Radiation Research Center (NSRRC), Hsinchu, Taiwan, provided beam time for the measurements of UPS and XPS.

## Conflict of Interest

The authors declare no conflict of interest.

## Keywords

graphene oxide, molybdenum oxide, nanoparticles, perovskite, solar cells

Received: May 9, 2018

Revised: July 3, 2018

Published online:

- 
- [1] F. Ye, H. Chen, F. Xie, W. Tang, M. Yin, J. He, E. Bi, Y. Wang, X. Yang, L. Han, *Energy Environ. Sci.* **2016**, *9*, 2295.
- [2] T. Liu, K. Chen, Q. Hu, R. Zhu, Q. Gong, *Adv. Energy Mater.* **2016**, *6*, 1600457.
- [3] T. Salim, S. Sun, Y. Abe, A. Krishna, A. C. Grimsdale, Y. M. Lam, *J. Mater. Chem. A* **2015**, *3*, 8943.
- [4] X. Yin, P. Chen, M. Que, Y. Xing, W. Que, C. Niu, J. Shao, *ACS Nano* **2016**, *10*, 3630.
- [5] H. Zhang, J. Cheng, F. Lin, H. He, J. Mao, K. S. Wong, A. K. Y. Jen, W. C. H. Choy, *ACS Nano* **2016**, *10*, 1503.
- [6] M.-H. Li, P.-S. Shen, K.-C. Wang, T.-F. Guo, P. Chen, *J. Mater. Chem. A* **2015**, *3*, 9011.
- [7] L. Meng, J. You, T.-F. F. Guo, Y. Yang, *Acc. Chem. Res.* **2015**, *49*, 155.
- [8] H. Kim, K.-G. Lim, T.-W. Lee, *Energy Environ. Sci.* **2016**, *9*, 12.
- [9] T. Umeyama, D. Matano, J. Baek, S. Gupta, S. Ito, V. Subramanian, H. Imahori, *Chem. Lett.* **2015**, *44*, 1410.
- [10] T. Umeyama, H. Imahori, *Dalton Trans.* **2017**, *46*, 15615.
- [11] P. Dhingra, P. Singh, P. J. S. Rana, A. Garg, P. Kar, *Energy Technol.* **2016**, *4*, 891.
- [12] F. Wang, M. Endo, S. Mouri, Y. Miyauchi, Y. Ohno, A. Wakamiya, Y. Murata, K. Matsuda, *Nanoscale* **2016**, *8*, 11882.
- [13] C.-C. Chung, S. Narra, E. Jokar, H.-P. Wu, E. Wei-Guang Diau, *J. Mater. Chem. A* **2017**, *5*, 13957.
- [14] Z. Wu, S. Bai, J. Xiang, Z. Yuan, Y. Yang, W. Cui, X. Gao, Z. Liu, Y. Jin, B. Sun, *Nanoscale* **2014**, *6*, 10505.
- [15] E. Jokar, Z. Y. Huang, S. Narra, C. Y. Wang, V. Kattoor, C. C. Chung, E. W. G. Diau, *Adv. Energy Mater.* **2018**, *8*, 1701640.
- [16] V. Georgakilas, J. N. Tiwari, K. C. Kemp, J. A. Perman, A. B. Bourlinos, K. S. Kim, R. Zboril, *Chem. Rev.* **2016**, *116*, 5464.
- [17] R. K. Singh, R. Kumar, D. P. Singh, *RSC Adv.* **2016**, *6*, 64993.
- [18] Q.-D. Yang, J. Li, Y. Cheng, H.-W. Li, Z. Guan, B. Yu, S.-W. Tsang, *J. Mater. Chem. A* **2017**, *5*, 9852.
- [19] K. C. Kwon, K. S. Choi, S. Y. Kim, *Adv. Funct. Mater.* **2012**, *22*, 4724.
- [20] J. Meyer, P. R. Kidambi, B. C. Bayer, C. Weijtens, A. Kuhn, A. Centeno, A. Pesquera, A. Zurutuza, J. Robertson, S. Hofmann, *Sci. Rep.* **2014**, *4*, 5380.
- [21] A. Kuruvilla, P. R. Kidambi, J. Kling, J. B. Wagner, J. Robertson, S. Hofmann, J. Meyer, *J. Mater. Chem. C* **2014**, *2*, 6940.
- [22] E. S. Choi, Y. J. Jeon, S. S. Kim, T. W. Kim, Y. J. Noh, S. N. Kwon, S. I. Na, *Appl. Phys. Lett.* **2015**, *107*, 023301.
- [23] N. T. Khoa, S. W. Kim, D. H. Yoo, E. J. Kim, S. H. Hahn, *Appl. Catal., A* **2014**, *469*, 159.
- [24] Z. Hu, C. Li, R. Nie, Y.-Q. Li, J.-X. Tang, X. Deng, *RSC Adv.* **2015**, *5*, 99431.
- [25] J.-T. Seo, J. Bong, J. Cha, T. Lim, J. Son, S. H. Park, J. Hwang, S. Hong, S. Ju, *J. Appl. Phys.* **2014**, *116*, 84312.
- [26] J. Liu, Y. Xue, Y. Gao, D. Yu, M. Durstock, L. Dai, *Adv. Mater.* **2012**, *24*, 2228.
- [27] Y. Jiang, C. Li, H. Liu, R. Qin, H. Ma, *J. Mater. Chem. A* **2016**, *4*, 9958.
- [28] M. Xiao, F. Huang, W. Huang, Y. Dkhissi, Y. Zhu, J. Etheridge, A. Gray-Weale, U. Bach, Y.-B. Cheng, L. Spiccia, *Angew. Chem., Int. Ed.* **2014**, *126*, 10056.
- [29] Z. Xiao, Q. Dong, C. Bi, Y. Shao, Y. Yuan, J. Huang, *Adv. Mater.* **2014**, *26*, 6503.
- [30] B. Chen, M. Yang, S. Priya, K. Zhu, *J. Phys. Chem. Lett.* **2016**, *7*, 905.
- [31] K. Wojciechowski, S. D. Stranks, A. Abate, G. Sadoughi, A. Sadhanala, N. Kopidakis, G. Rumbles, C. Z. Li, R. H. Friend, A. K. Y. Jen, H. J. Snaith, *ACS Nano* **2014**, *8*, 12701.
- [32] W. Zhang, M. Saliba, S. D. Stranks, Y. Sun, X. Shi, U. Wiesner, H. J. Snaith, *Nano Lett.* **2013**, *13*, 4505.
- [33] L. L. Li, Y. C. Chang, H. P. Wu, E. W. G. Diau, *Int. Rev. Phys. Chem.* **2012**, *31*, 420.